NANO LETTERS

Letter

pubs.acs.org/NanoLett

3D Imaging of Twin Domain Defects in Gold Nanoparticles

Andrew Ulvestad,*[,†] Jesse N. Clark,[‡,§] Ross Harder,[∥] Ian K. Robinson,[⊥,▽] and Oleg G. Shpyrko[†]

[†]Department of Physics, University of California-San Diego, La Jolla, California 92093-0319, United States

[‡]Stanford PULSE Institute, SLAC National Accelerator Laboratory, Menlo Park, California 94025, United States

[§]Center for Free-Electron Laser Science (CFEL), Deutsches Elektronensynchrotron (DESY), Notkestrasse 85, 22607 Hamburg, Germany

[∥]Advanced Photon Source, Argonne National Laboratory, Argonne, Illinois 60439, United States

[⊥]London Center for Nanotechnology, University College London, London WC1E 6BT, United Kingdom

[▽]Research Complex at Harwell, Didcot, Oxfordshire OX11 0DE, United Kingdom

Supporting Information

ABSTRACT: Topological defects are ubiquitous in physics and include crystallographic imperfections such as defects in condensed matter systems. Defects can determine many of the material's properties, thus providing novel opportunities for defect engineering. However, it is difficult to track buried defects and their interfaces in three dimensions with nanoscale resolution. Here, we report three-dimensional visualization of gold nanocrystal twin domains using Bragg coherent X-ray diffractive imaging in an aqueous environment. We capture the size and location of twin domains, which appear as voids in the Bragg electron density, in addition to a component of the strain field. Twin domains can interrupt the stacking order of the parent crystal, leading to a phase offset between the separated parent crystal pieces. We utilize this phase offset to estimate the roughness of the twin boundary. We measure the diffraction signal from the crystal twin and show its Bragg electron density fits into the parent crystal void. Defect imaging will likely facilitate improvement and rational design of nanostructured materials.

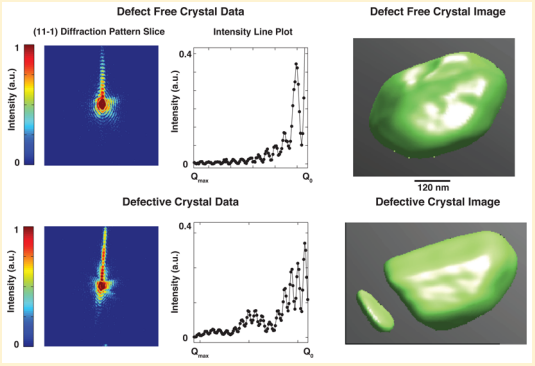

KEYWORDS: *coherent imaging, twin domain, defects, gold nanoparticle, X-ray imaging*

Many nanostructured materials show novel properties relative to their bulk counterparts, including size-tunable thermodynamics, crystallographic facet dependent kinetics, and extended life cycles.[1] Defects, or crystallographic imperfections, can further alter these properties.[2−4] For example, screw dislocations can act as fast hydrogen diffusion channels in palladium nanocrystals during the hydriding phase transformation[5] and twin domains can enhance photocatalytic activity.[6] Twin domains are important in many technological and fundamental challenges,[7] including enhanced hardening of stainless steel,[8] understanding plastic deformation mechanisms,[9] and hydrogen embrittlement.[10] Motivated by the opportunity for defect engineering, many researchers worked to develop imaging techniques capable of resolving defects. Recently, electron tomography was used to visualize the 3D structure of a ten-nanometer gold nanoparticle and identified twinned regions of the crystal.[11,12] Another technique challenged the theoretical and experimental assumption that coherent twin boundaries are always perfectly flat interfaces.[13] Here, we show that coherent X-ray diffractive imaging (CXDI) is particularly sensitive to defects and can resolve their full 3D structure nondestructively for thick samples in macroscopic amounts of electrolyte thereby accessing a previously unexplored area.

Coherent X-ray diffraction imaging in Bragg geometry is a powerful tool that uses interference produced by coherent X-rays coupled with phase retrieval algorithms to reconstruct the 3D electron density and atomic displacement fields in nanocrystals.[14−22] The primary advantage CXDI provides over other imaging techniques is the ability to image, nondestructively, both the electron density, typically with a resolution of tens of nanometers, and the displacement field, with subangstrom resolution, in full 3D detail for thick (>100 nm) samples immersed in realistic sample environments. Thus, it can be used to study buried defects and interfaces with great precision.

A CXDI measurement consists of aligning and centering a nanocrystal in the focused beam. In this case, the nanocrystal was on a silicon substrate. An area detector (such as a charge-coupled device (CCD)) is then placed far enough away from the crystal to satisfy the "far field" condition and to ensure the diffraction pattern is oversampled by at least a factor of 2. The crystal is then rotated in small steps[23,24] and the individual 2D patterns stacked together to form a 3D data set.[25,26] The data set is inverted using

Received: March 20, 2015
Revised: May 8, 2015
Published: May 12, 2015

DOI: 10.1021/acs.nanolett.5b01104
Nano Lett. 2015, 15, 4066−4070

phase retrieval algorithms to produce a real space image that is, in general, complex. The real part corresponds to the electron density from the atomic planes in the particular Bragg orientation (hereafter referred to as the Bragg electron density).[27] This point is essential as it shows that pieces of a crystal not satisfying the chosen Bragg condition, for example, twin domains, will be invisible in the retrieved Bragg electron density maps. The imaginary part is related to the displacement field, **u**, via $\phi = \boldsymbol{G} \cdot \boldsymbol{u}$, where **G** is the scattering vector. In this particular case, $\phi = G_{11-1}u_{11-1}$, and a phase value of 2π corresponds to a displacement of one d_{11-1} spacing.[24] Thus, a phase of 0.5 rad, which is reproducible in the reconstructions, translates into a subangstrom displacement. The strain is then determined to better than 10^{-4}.[28] . How accurately that value can be placed to specific spatial locations within the reconstruction is given by the phase retrieval transfer function. For further experimental details, please see Supporting Information Methods.

Twin domains occur when two crystals share some of the same crystal lattice points and are related by a symmetry operation. In the face centered cubic structure, the packing of {111} crystallographic planes proceeds in ABC ordering. A crystal twin would share one of these planes, say C, but follow a mirrored packing order, for example CBA, which is the mirror of the previous sequence. Thus, a crystal with a strain-free twin domain can be formed via the sequence ABCABC**BACB**ABCABC in which the underlined text indicate the shared planes and the bold letters indicate the planes belonging to the twinned crystal. We distinguish these from deformation faults, which are slips that maintain orientation, for example, ABCABC|BCABCABC. The twin crystal planes are rotated with respect to the parent crystal lattice and, thus, will appear as a missing Bragg electron density in particular Bragg reflections. To investigate the possibility of twin domains in gold nanoparticles, we compared the coherent X-ray diffraction data from two different crystals.

Figure 1a–d shows experimental data for two gold nanocrystal in an aqueous environment using a liquid flow cell as shown in Supporting Information Figure S1. Figure 1a is the log of a 2D slice of the 3D Bragg reflection (see Supporting Information Figure S2 for a 3D rendering of the diffraction data showing Figure 2a cross-section location). Figure 1b shows the fringe modulation from the finite size of the nanocrystal as well as the decay of the fringe intensity as a function of Q, the reciprocal space coordinate. Q_{max} corresponds to spatial length of 6 nm, whereas Q_1 is near the center of the Bragg peak. This data is consistent with a crystal that has no defects (visible at our resolution) affecting the (11−1) crystallographic planes. Figure 1c,d, corresponding to another crystal, is different. A clear enveloping in fringe intensity is seen both in Figure 1c and in Figure 1d, which is attributed to (potentially multiple) missing sections of Bragg electron density in the (11−1) crystallographic planes. For the case of a single twin domain, an analogy can be drawn between the diffraction pattern and the double slit experiment. The missing Bragg electron density gives rise to interference between the two crystal pieces leading to an enveloping of the intensity, as is the case for double slit diffraction. To verify this relationship and view the defect in real space, we performed phase retrieval[25,29−31] on the 3D diffraction data sets (see Supporting Information Methods for details). For recent progress in phase retrieval, see refs 23 and 32−35.

Figure 2a,b shows the Bragg electron density of the crystal in real space as a green isosurface drawn at 35%, whereas the assumed location of the substrate is shown in black. Recall that the Bragg electron density is the electron density recovered from

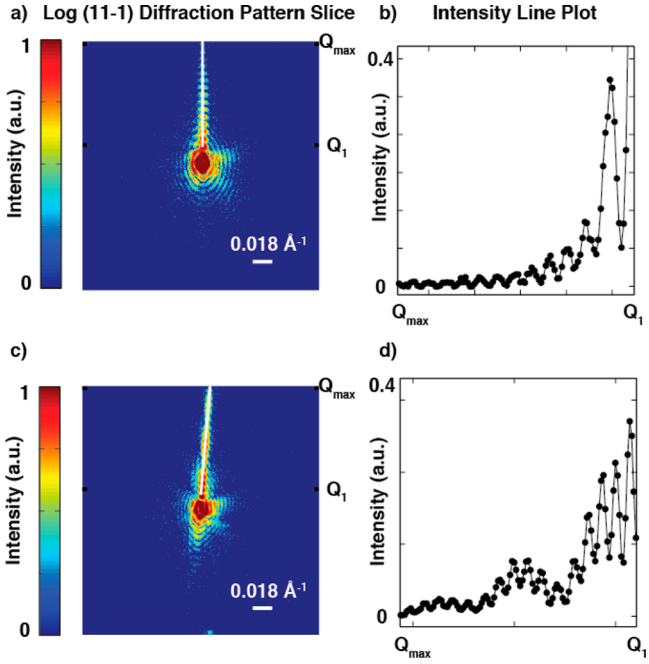

Figure 1. Coherent X-ray diffraction data for two representative nanocrystals. (a) 2D slice of the log of the (11−1) Bragg reflection from a single gold nanocrystal in solution showing a clear fringe pattern with decaying intensity. (b) Line plot along the white line drawn in panel a of the intensity along the fringes. (c)−(d) Same as above, but for a different crystal with a noticeably different intensity profile.

measuring a particular Bragg peak. While the physical electron density is approximately homogeneous over the sample, the Bragg electron density will show voids when subsets of the measured planes are rotated out of the Bragg condition. The defect-free crystal has a six-sided shape consistent with electron microscopy images (Supporting Information Figures S3 and S4) and a continuous Bragg electron density determined with 12 nm resolution as defined by the phase retrieval transfer function (Supporting Information Figure S5). The defective crystal has a region of approximately 100 nm of missing Bragg electron density as evident by the gap between green isosurfaces (drawn at a 35% level) in Figure 2b (for a slice showing the magnitude of the retrieved Bragg electron density, see Supporting Information Figure S6). The missing region must be rotated out of the (11−1) Bragg condition. Two separated nanocrystals in exactly the same orientation could explain this result but are not seen in scanning electron microscopy (SEM) images (Supporting Information Figure S1). In addition, this scenario is extremely unlikely due to the sensitivity of the Bragg condition to the particle's orientation. Although we focus on the case of a single twin domain here, Supporting Information Figure S7 shows a more complicated example. If the twin domains are smaller than the resolution (12 nm) then they cannot be faithfully reconstructed. However, in principle, all possible combinations are distinctly encoded into the diffraction pattern (see Supporting Information Figure S8 for three examples). To further understand the defect, the displacement field inside the nanocrystal was investigated.

Figure 3a shows a central cross-section taken perpendicular to the substrate of the phase inside the defective nanocrystal shown in Figure 2b. A displacement field pixel with a value of 1.07 rad, for example, indicates that the unit cells in this location are displaced from their equilibrium positions on average by 0.4 Å in

DOI: 10.1021/acs.nanolett.5b01104
Nano Lett. 2015, 15, 4066−4070

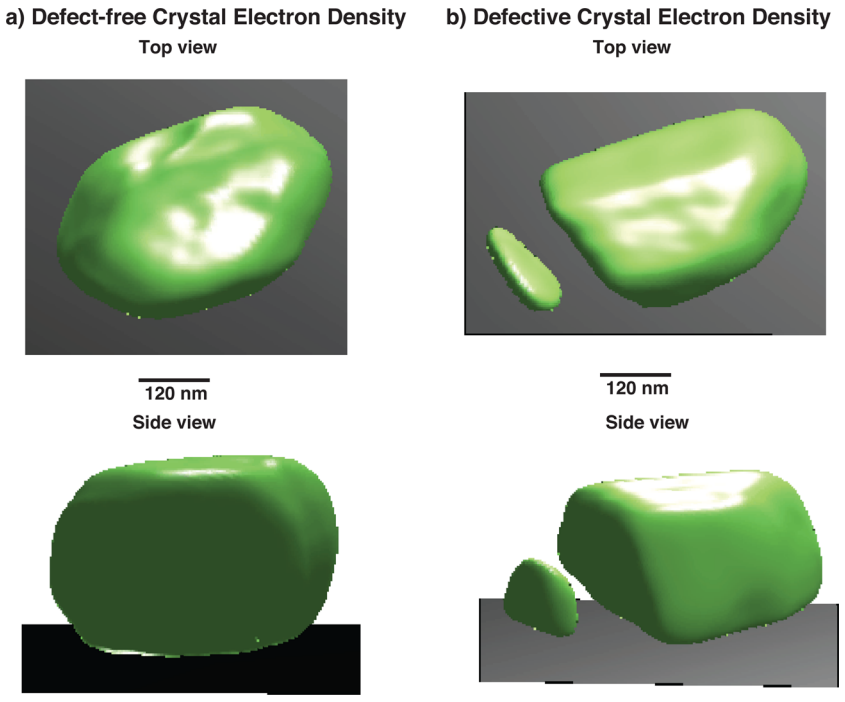

Figure 2. Electron density isosurface for a defect-free and defective crystal. (a) Two different views of a defect-free crystal represented by a green isosurface drawn at 35%, whereas the substrate is represented as a black plane. (b) Defective crystal represented by a green isosurface that shows a region of missing electron density. The assumed substrate location is shown in black.

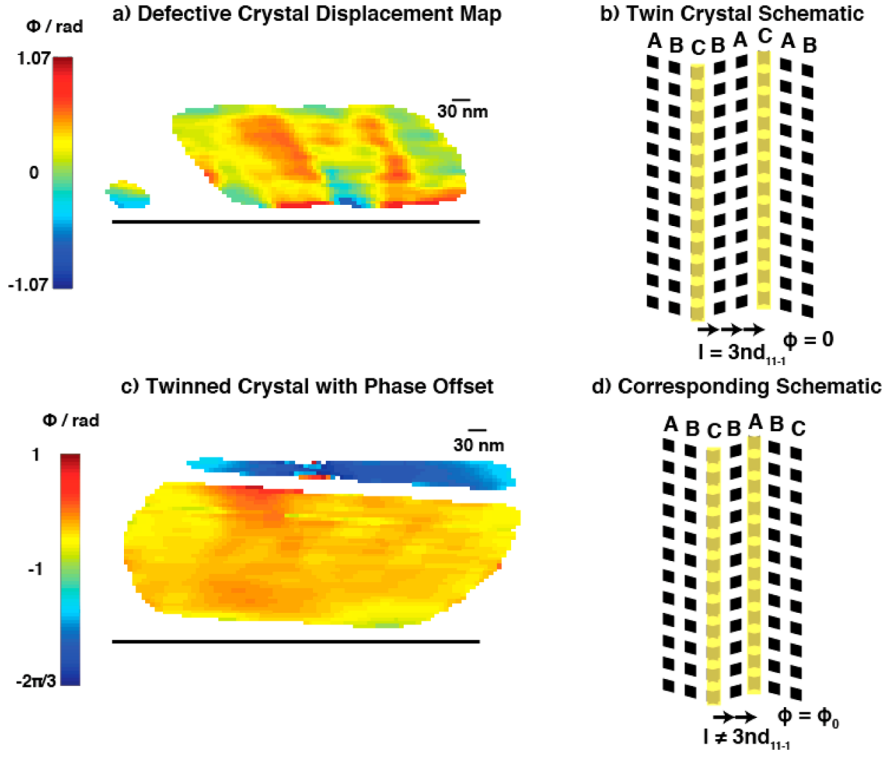

Figure 3. Atomic displacement map and twin crystal schematic for two crystals. (a) Central cross section taken perpendicular to the substrate of the phase, which is proportional to the u_{11-1} displacement field, for the defective crystal shown in Figure 2b. (b) Schematic of the twin domain responsible for the missing electron density. The stacking sequence is shown and the yellow highlighted planes are coherent interfaces. The width of the crystal twin is such that the spacing, *l*, is an integer multiple of three d_{11-1} as no phase offset is seen. (c) Atomic displacement map in radians for a different crystal. A phase offset in the disconnected piece of the parent crystal is visible.

the [11−1] direction. There are no edge or screw dislocations evident in this projection of the displacement field.[36,37] There is also no rapid displacement variation near the boundary of the missing Bragg electron density, indicating small strain. Thus, the defect boundary is likely a coherent, meaning both the parent and twin share the atomic planes at the interface. Figure 3b shows a

DOI: 10.1021/acs.nanolett.5b01104
Nano Lett. 2015, 15, 4066−4070

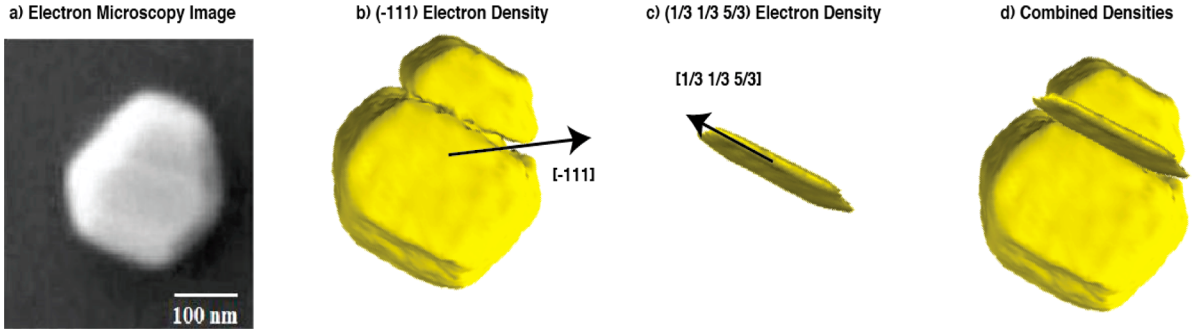

Figure 4. Measurement of a Crystal and its Twin. (a) Electron microscopy image of the gold nanocrystal measured with CXDI. (b) Bragg electron density isosurface drawn at a 35% level from the (−111) Bragg peak measurement. (c) Bragg electron density isosurface measured from the twin crystal at (1/3 1/3 5/3), whose density is missing in panel b. (d) Densities overlaid produce a uniform crystal. The twin crystal is indexed in the parent crystal's reciprocal lattice, which gives fractional Bragg peak indices as expected.

schematic of a crystal twin that generates a missing region of Bragg electron density in a strain free fashion. The crystal twin is a mirror image of the original crystal and has stacking order CBA. It forms two coherent interfaces with the original crystal that are strain free. Its width, l, must be an integer, n, multiple of three d_{11-1}, where d_{11-1} is the distance between (11−1) atomic planes, due to the approximately zero phase offset observed between the parent and disconnected crystal pieces. Figure 3c−d reveal a different case in which the disconnected piece is phase offset from the parent crystal. We utilized the average and standard deviation of the phase offsets to gain information about the roughness of the coherent twin boundary.

Consider an atomically flat twin boundary that breaks the stacking order between two pieces of a parent crystal. The disconnected piece of the parent crystal in the absence of any other effects should have a uniform phase offset that is set by the twin width. However, it was shown that twin boundary interfaces are seldom perfect,[13] which implies the phase offset of the disconnected piece is actually a sum of phase offsets corresponding to different twin crystal widths: $l = 3nd_{11-1}$ (0 phase offset), $l = (3n + 1)d_{11-1}$ ($2\pi/3$ offset), $l = (3n + 2)d_{11-1}$ ($4\pi/3$ offset) for n an integer. Thus, the standard deviation of the phase is related to the roughness or variation of the twin width along the interface. We are insensitive to roughness jumps of $l = (3n + 3)d_{11-1}$, which yields no offset.

The parent crystal in Figure 3b has an average and standard deviation of $\varphi_0 = 0.37 \pm 0.37$ rad, whereas the disconnected piece has $\varphi_0 = 0.43 \pm 0.24$ rad. We thus conclude that the interface is nearly flat as the differential offset between the two pieces is very close to zero. For the reconstruction shown in Figure 3c, the phase offset for the parent piece is approximately zero while for the disconnected piece it is $\varphi_0 = -2.23 \pm 0.46$ rad. The expected value from a twin of width $l = (3n + 1)d_{11-1}$ and perfectly flat interfaces is $-2\pi/3$ or −2.09 rad. This surface, thus, is likely more rough, due to additional jogs and kinks, due to the larger discrepancy between the calculated and measured values. Note, however, that strain will also contribute to phase variations.

To completely characterize the crystal structure, three or more independent Bragg peaks must be measured.[38−40] This ensures that any defects present are discovered, as defects in certain orientations do not affect certain Bragg reflections, for example, the defect-free crystal discussed in Figure 2a could have a defect that is invisible in the (11−1) Bragg planes.

In the following discussion, a patterned gold nanocrystal sample (see Supporting Information Figure S2 and Methods) was used that makes comparison with an electron microscopy image of the same crystal facile. The rotated, faulted twin domains are indexed in the coordinate frame of the parent crystal. A mirror of the f.c.c. reciprocal lattice around the [−111] direction maps the other {−111} lattice points onto permutations of {1/3, 1/3, 5/3}. We first located the (−111) and (200) reflections from a single gold nanocrystal using a confocal microscope to align the crystal to the center of rotation of the diffractometer.[40−44] These motor positions were input into the beamline control software (SPEC) that then calculated the position to measure the (1/3 1/3 5/3) Bragg peak, corresponding to the twin portion of the crystal.

Figure 4a shows an electron microscopy image of a gold nanocrystal on a patterned substrate. A defect is visible as a slight contrast change in the SEM image. Figure 4b shows the Bragg electron density isosurface drawn at a 35% level resulting from measurement of the (−111) Bragg peak. The defective region is shown quite clearly as a region of missing Bragg electron density. Figure 4c is the Bragg electron density corresponding to the (1/3 1/3 5/3) Bragg peak, which has a fractional index due to the mirroring of the twin and parent crystal lattices. For slices of the twin diffraction data and Bragg electron density, see Supporting Information Figure S9. The size and shape of the crystal twin's Bragg electron density in Figure 4c fit into the void in Figure 4b as shown in Figure 4d. This is final confirmation that the defect visible in the diffraction data is indeed a crystal twin formed in a strain free fashion.

We studied topological defects in gold nanoparticles using coherent X-ray diffractive imaging. The 3D defects we observe appear as regions of missing Bragg electron density and show little strain at the boundaries between the crystal and the defect. Thus, we conclude that twin domains are responsible. The twin domain widths cause discrete phase offsets between the pieces of the parent crystal. We use this fact to estimate the twin/parent crystal interface roughness. We show twin domains themselves can be measured by CXDI and their electron densities fit into the parent crystal voids. Our results show CXDI is a powerful tool for understanding defects and can potentially aid in the design of mechanical, electronic, and optical properties of nanocrystals.

■ ASSOCIATED CONTENT

Supporting Information

Sample synthesis, experimental method, and phase retrieval details are described in additional detail. Four additional figures are provided showing sample SEMs, the aqueous cell, and the resolution. The Supporting Information is available free of charge

DOI: 10.1021/acs.nanolett.5b01104
Nano Lett. 2015, 15, 4066−4070

on the ACS Publications website at DOI: 10.1021/acs.nanolett.5b01104.

AUTHOR INFORMATION

Corresponding Author

*E-mail: aulvesta@ucsd.edu.

Author Contributions

A.U., J.N.C., R.H., and I.K.R. conducted the experiments and performed the data analysis. A.U. wrote the paper. All authors interpreted the results and revised the manuscript.

Notes

The authors declare no competing financial interest.

ACKNOWLEDGMENTS

This work was supported by U.S. Department of Energy, Office of Science, Office of Basic Energy Sciences, under Contract DE-SC0001805. I.K.R., R.H., and J.N.C. acknowledge support from EPSRC grant EP/I022562/1 and an ERC Advanced Grant 227711 "nanosculpture". J.N.C. gratefully acknowledges financial support from the Volkswagen Foundation. This research used resources of the Advanced Photon Source, a U.S. Department of Energy (DOE) Office of Science User Facility operated for the DOE Office of Science by Argonne National Laboratory under Contract No. DE-AC02-06CH11357. We thank the staff at Argonne National Laboratory and the Advanced Photon Source for their support. We also thank Dr. Andrej Singer for useful discussion regarding twinning in face centered cubic crystals.

ABBREVIATIONS

3D, three-dimensional; CXDI, coherent X-ray diffractive imaging; CCD, charge-coupled device; SEM, scanning electron microscopy

REFERENCES

(1) Bardhan, R.; Hedges, L. O.; Pint, C. L.; Javey, A.; Whitelam, S.; Urban, J. J. *Nat. Mater.* **2013**, *12*, 905−912.

(2) Banhart, F.; Kotakoski, J.; Krasheninnikov, A. V. *ACS Nano* **2011**, *5*, 26−41.

(3) Turner, S.; Buseck, P. R. *Nature* **1983**, *304*, 143−146.

(4) Abbey, B. *J. Met.* **2013**, *65*, 1183−1201.

(5) Walker, A. M.; Slater, B.; Gale, J. D.; Wright, K. *Nat. Mater.* **2004**, *3*, 715−720.

(6) Liu, M.; Jing, D.; Zhou, Z.; Guo, L. *Nat. Commun.* **2013**, *4*, 2278.

(7) Chen, Y.; Yu, K. Y.; Liu, Y.; Shao, S.; Wang, H.; Kirk, M. a.; Wang, J.; Zhang, X. *Nat. Commun.* **2015**, *6*, 7036.

(8) Zhang, X.; Misra, a.; Wang, H.; Shen, T. D.; Nastasi, M.; Mitchell, T. E.; Hirth, J. P.; Hoagland, R. G.; Embury, J. D. *Acta Mater.* **2004**, *52*, 995−1002.

(9) Li, N.; Wang, J.; Misra, a.; Zhang, X.; Huang, J. Y.; Hirth, J. P. *Acta Mater.* **2011**, *59*, 5989−5996.

(10) Seita, M.; Hanson, J. P.; Gradečak, S.; Demkowicz, M. J. *Nat. Commun.* **2015**, *6*, 6164.

(11) Scott, M. C.; Chen, C.-C.; Mecklenburg, M.; Zhu, C.; Xu, R.; Ercius, P.; Dahmen, U.; Regan, B. C.; Miao, J. *Nature* **2012**, *483*, 444−447.

(12) Chen, C.-C.; Zhu, C.; White, E. R.; Chiu, C.-Y.; Scott, M. C.; Regan, B. C.; Marks, L. D.; Huang, Y.; Miao, J. *Nature* **2013**, *496*, 74−77.

(13) Wang, Y. M.; Sansoz, F.; LaGrange, T.; Ott, R. T.; Marian, J.; Barbee, T. W.; Hamza, A. V. *Nat. Mater.* **2013**, *12*, 697−702.

(14) Ulvestad, A.; Singer, A.; Cho, H.-M.; Clark, J. N.; Harder, R.; Maser, J.; Meng, Y. S.; Shpyrko, O. G. *Nano Lett.* **2014**, *14*, 5123−5127.

(15) Robinson, I.; Harder, R. *Nat. Mater.* **2009**, *8*, 291−298.

(16) Clark, J. N.; Huang, X.; Harder, R.; Robinson, I. K. *Nat. Commun.* **2012**, *3*, 993.

(17) Ulvestad, A.; Cho, H. M.; Harder, R.; Kim, J. W.; Dietze, S. H.; Fohtung, E.; Meng, Y. S.; Shpyrko, O. G. *Appl. Phys. Lett.* **2014**, *073108*, 2−6.

(18) Clark, J. N.; Beitra, L.; Xiong, G.; Higginbotham, a; Fritz, D. M.; Lemke, H. T.; Zhu, D.; Chollet, M.; Williams, G. J.; Messerschmidt, M.; Abbey, B.; Harder, R. J.; Korsunsky, a M.; Wark, J. S.; Robinson, I. K. *Science* **2013**, *341*, 56−59.

(19) Singer, A.; Ulvestad, A. P.; Cho, H.-M.; Kim, J. W.; Maser, J.; Harder, R.; Meng, Y. S.; Shpyrko, O. G. *Nano Lett.* **2014**, *14*, 5295−5300.

(20) Leake, S. J.; Newton, M. C.; Harder, R.; Robinson, I. K. *Opt. Express* **2009**, *17*, 15853−15859.

(21) Minkevich, a. a.; Fohtung, E.; Slobodskyy, T.; Riotte, M.; Grigoriev, D.; Schmidbauer, M.; Irvine, a. C.; Novák, V.; Holý, V.; Baumbach, T. *Phys. Rev. B* **2011**, *84*, 054113.

(22) Kim, J. W.; Manna, S.; Dietze, S. H.; Ulvestad, a.; Harder, R.; Fohtung, E.; Fullerton, E. E.; Shpyrko, O. G. *Appl. Phys. Lett.* **2014**, *105*, 173108.

(23) Minkevich, a. a.; Köhl, M.; Escoubas, S.; Thomas, O.; Baumbach, T. *J. Synchrotron Radiat.* **2014**, *21*, 1−10.

(24) Robinson, I. *J. Phys. Soc. Jpn.* **2012**, *82*, 21012.

(25) Marchesini, S.; He, H.; Chapman, H. *Phys. Rev. B* **2003**, 1−5.

(26) Shechtman, Y.; Eldar, Y. C.; Cohen, O.; Chapman, H. N.; Miao, J. *IEEE Signal Proc. Mag.* **2015**, 87−109.

(27) Vartanyants, I. A.; Oleksandr, Y. *X-ray Diffraction: Modern Experimental Techniques*; Seeck, O. H.; Murphy, B. M., Eds.; Pan Stanford: Singapore, 2013; pp 1−51.

(28) Yang, W.; Huang, X.; Harder, R.; Clark, J. N.; Robinson, I. K.; Mao, H. *Nat. Commun.* **2013**, *4*, 1680.

(29) Fienup, J. R.; Wackerman, C. C.; Arbor, A. *J. Opt. Soc. Am. A* **1986**, *3*, 1897−1907.

(30) Fienup, J. R. *Appl. Opt.* **1982**, *21*, 2758−2769.

(31) Fienup, J. R.; Kowalczyk, A. M. *J. Opt. Soc. Am. A* **1990**, *7*, 450.

(32) Marchesini, S. *Rev. Sci. Instrum.* **2007**, *78*, 011301.

(33) Marchesini, S. *J. Opt. Soc. Am. A* **2007**, *24*, 3289−3296.

(34) Köhl, M.; Minkevich, a. a.; Baumbach, T. *Opt. Express* **2012**, *20*, 17093.

(35) Adams, D. E.; Martin, L. S.; Seaberg, M. D.; Gardner, D. F.; Kapteyn, H. C.; Murnane, M. M. *Opt. Express* **2012**, *20*, 24778.

(36) Takahashi, Y.; Suzuki, A.; Furutaku, S.; Yamauchi, K.; Kohmura, Y.; Ishikawa, T. *Phys. Rev. B* **2013**, *87*, 121201.

(37) Clark, J. N.; Ihli, J.; Schenk, A. S.; Kim, Y.; Kulak, A. N.; Campbell, M.; Nisbit, G.; Meldrum, F. C.; Robinson, I. K. 1−23 arXiv:1501.02853.

(38) Pfeifer, M. A.; Williams, G. J.; Vartanyants, I. A.; Harder, R.; Robinson, I. K. *Nature* **2006**, *442*, 63−66.

(39) Newton, M. C.; Leake, S. J.; Harder, R.; Robinson, I. K. *Nat. Mater.* **2010**, *9*, 120−124.

(40) Beitra, L.; Watari, M.; et al. *AIP Conf. Proc.* **2010**, *1234*, 57.

(41) Tesler, A. B.; Maoz, B. M.; Feldman, Y.; Vaskevich, A.; Rubinstein, I. *J. Phys. Chem. C* **2013**, *117*, 11337−11346.

(42) Müller, C. M.; Mornaghini, F. C. F.; Spolenak, R. *Nanotechnology* **2008**, *19*, 485306.

(43) Chen, C.-C.; Miao, J.; Wang, C.; Lee, T. *Phys. Rev. B* **2007**, *76*, 064113.

(44) Vartanyants, I.; Robinson, I. *J. Phys.: Condens. Matter* **2001**, *13*, 10593.

DOI: 10.1021/acs.nanolett.5b01104
Nano Lett. 2015, 15, 4066−4070